Supplementary Information For:

Oxygen Enhanced- and Dynamic Contrast Enhanced- Optoacoustic Tomography provide surrogate biomarkers of tumour vascular function, hypoxia and necrosis.

Authors: M R Tomaszewski[1,2], M Gehrung[1,2,3], J Joseph[1,2], I Quiros-Gonzalez[1,2], J A Disselhorst[3] and S E Bohndiek[1,2] *

Affiliations: [1]Department of Physics and [2]Cancer Research UK Cambridge Institute, University of Cambridge, [3]Werner Siemens Imaging Center, Preclinical Imaging and Radiopharmacy, University of Tuebingen, Germany

Supplementary Figure S1 **Diagram of the optoacoustic scan timeline**

50:50 Air:O_2	**Medical air (21% O_2)**		**100% O_2**	**Medical air (21% O_2)**
Anaesthesia induction and animal preparation **5 min**	Temperature stabilisation in the scanner **15 min**	Medical air to 100% Oxygen after 3 minutes OE-OT scan **8 min**	100% Oxygen to medical air after 3 minutes OE-OT scan **8 min**	DCE-OT scan ICG injection after 1 minute **15 min**

Imaging followed by sacrifice, rapid tumour excision and fixation for histological analysis within 10 minutes

Supplementary Figure S2. **CAIX staining shows co-localisation to pimonidazole hypoxia staining in PC3 tumours.** Consecutive sections from a representative PC3 tumour stained with CAIX (left) and pimonidazole (right) show very similar staining patterns, indicating that CAIX staining in PC3 tumours may be indicative of hypoxia.

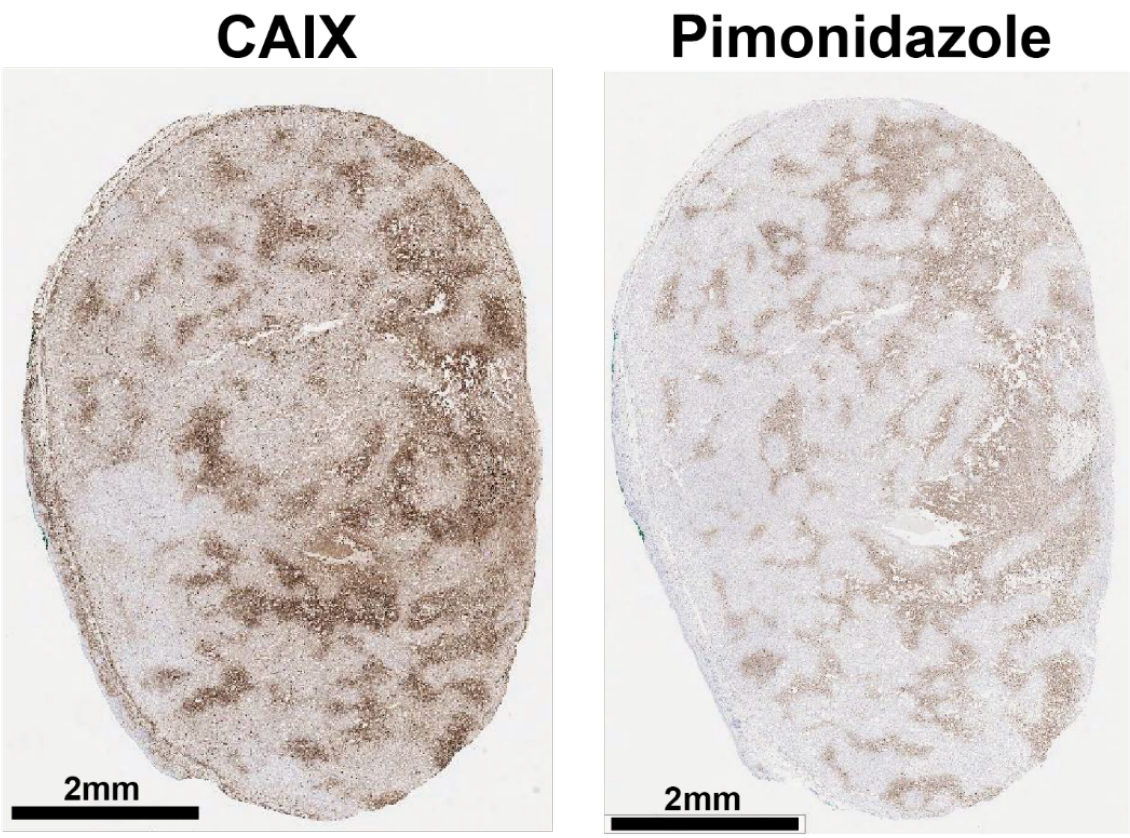

Supplementary Figure S3. **Demonstration of responding fraction binarisation for metric extraction.** Maps of OE-OT ΔSO_2^{MSOT} and DCE-OT ΔICG (left) were compared with maps of standard deviation of the baseline variation in SO_2^{MSOT} and ICG signals (centre) and the pixels showing enhancement that exceeded 2x the standard deviation threshold were classified as responding (right). The ratio of responding tumour pixels to all tumour pixels defines the Responding Fraction (RF). Example images from PC3 tumours.

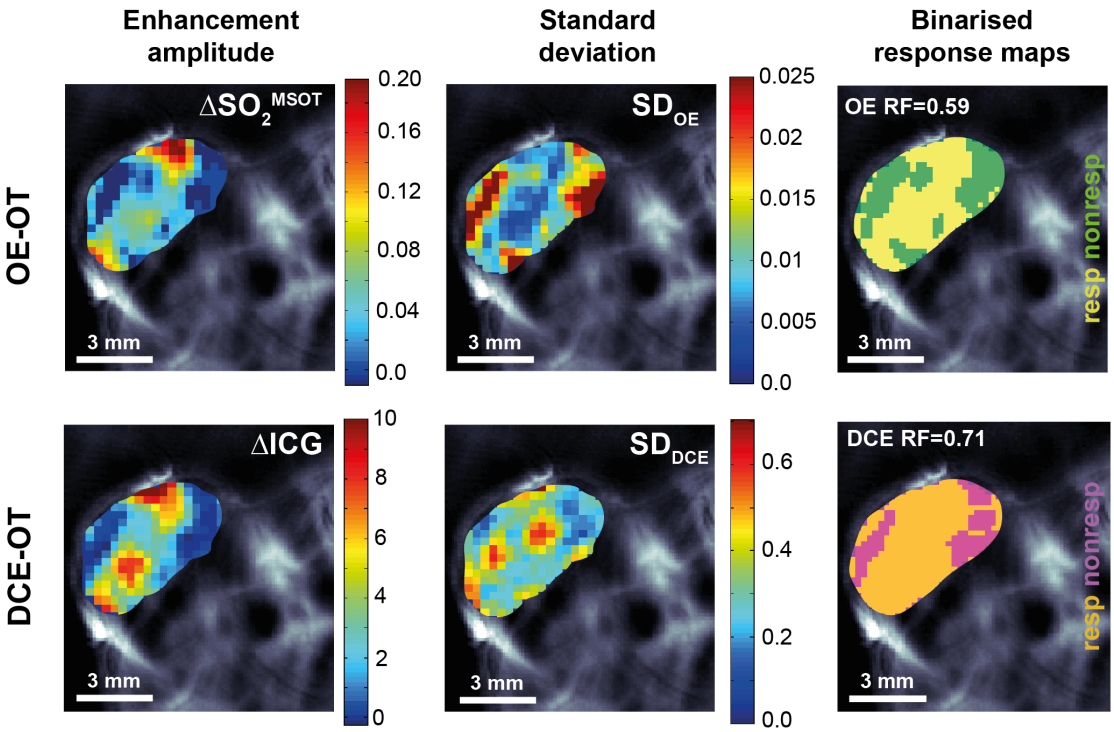

Supplementary Figure S4 **Schematic layer architecture for the Convolution Neural Networks based model for necrosis identification in H&E sections.** Example images from PC3 tumours.

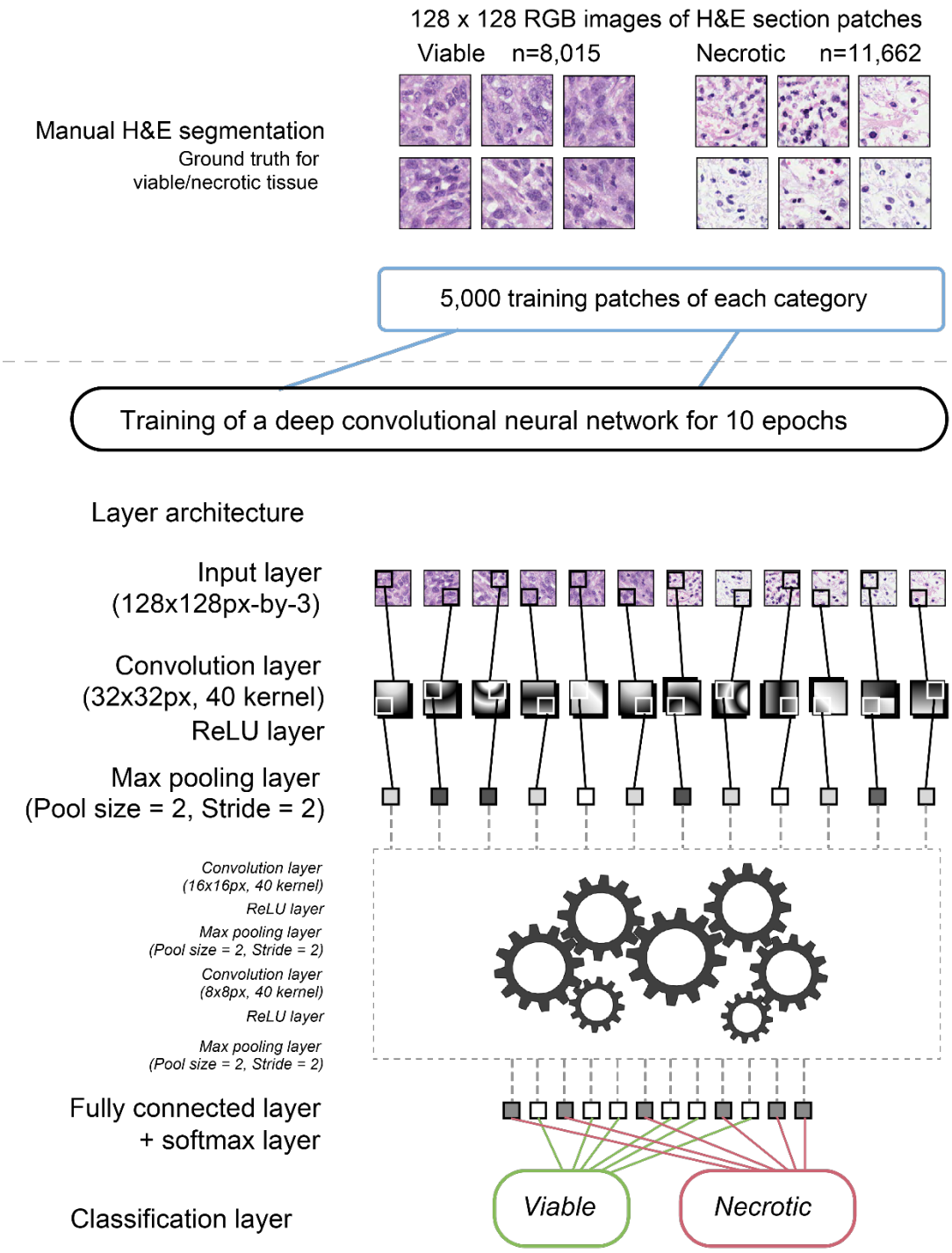

Supplementary Figure S5 **Examples of the necrosis identification algorithm performance.** Necrotic regions were manually identified in 3 example H&E sections (A), as highlighted by red circles. The Convolution Neural Network based model (B) as used in the study was found to correctly identify all the necrotic and viable regions of the tissue. Example images from PC3 tumours.

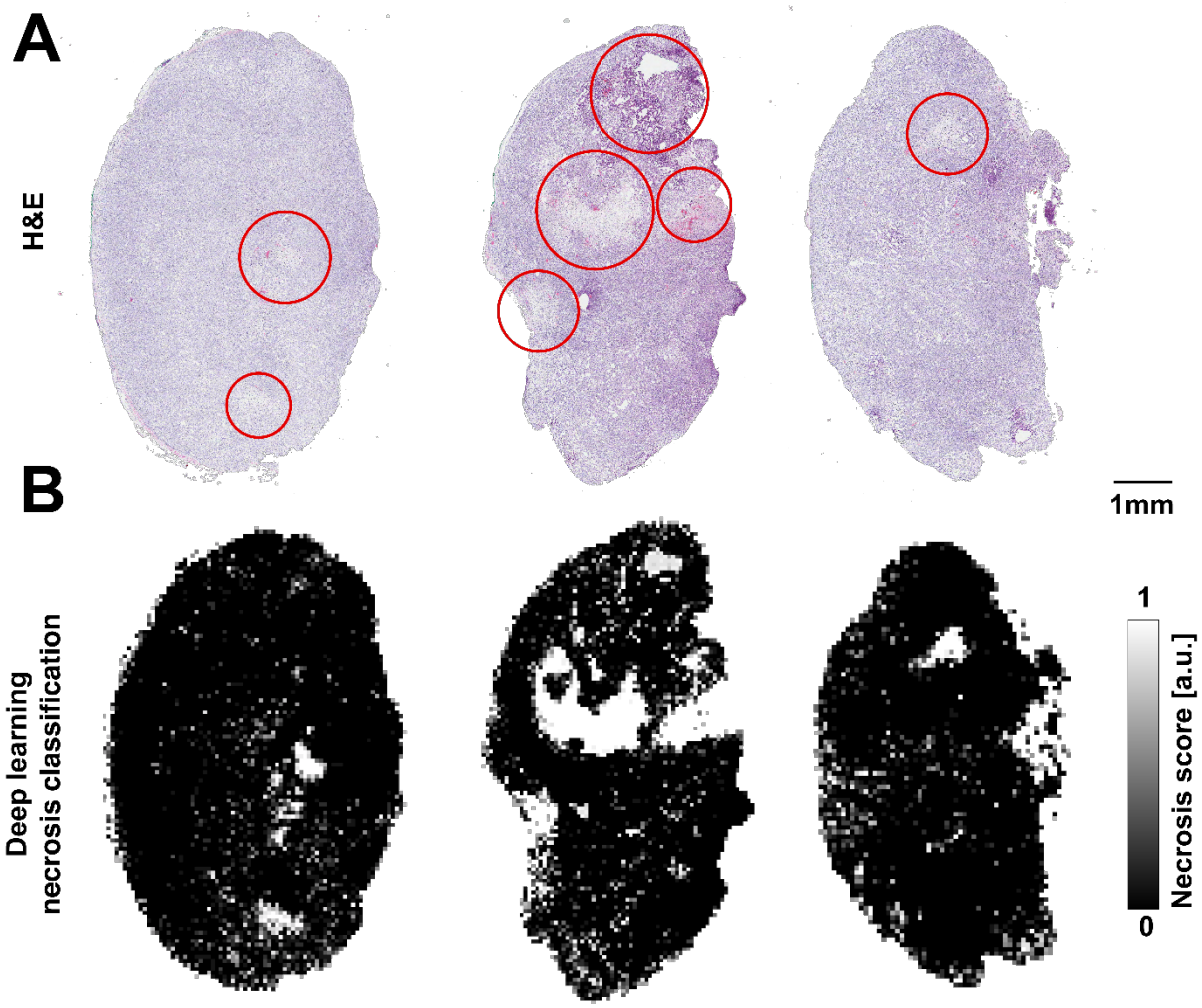

Supplementary Figure S6. **Convolution Neural Network (CNN) based model accurately identifies tissue necrosis.** Strong positive correlation was observed between the necrotic area fraction as quantified by CNN based model, and by manual identification of necrotic areas. n=18 PC3 tumours, * p<0.05, ** p<0.01, *** p<0.001

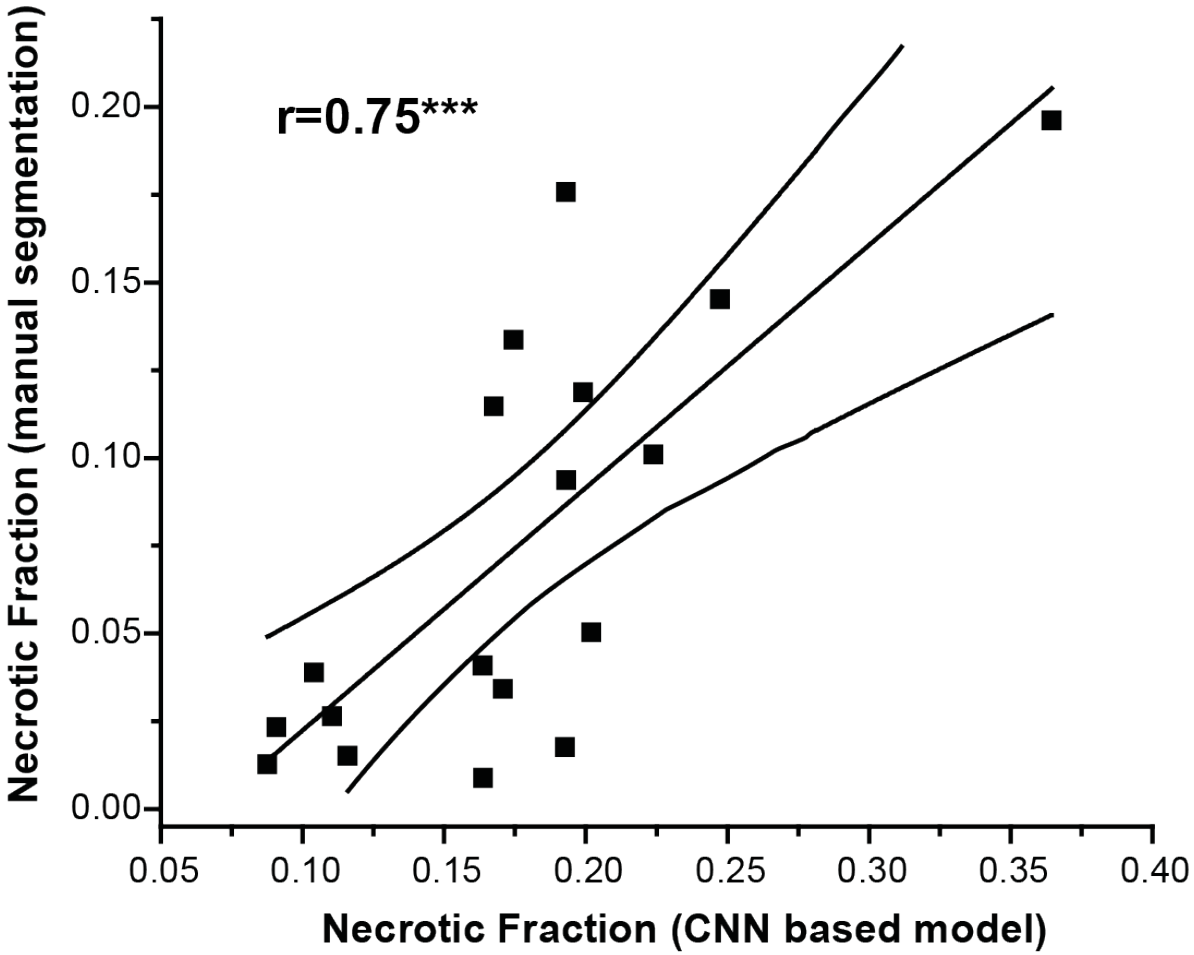

Supplementary Figure S7. **Hypoxic tumours show weak OE-OT and DCE-OT response.** Representative PC3 tumours with low (left) and high (right) CAIX staining (A) show differences in the amplitude of OE and DCE-OT responses (B), which translate to low OE and DCE RF in the binarised response of highly hypoxic tumours (C).

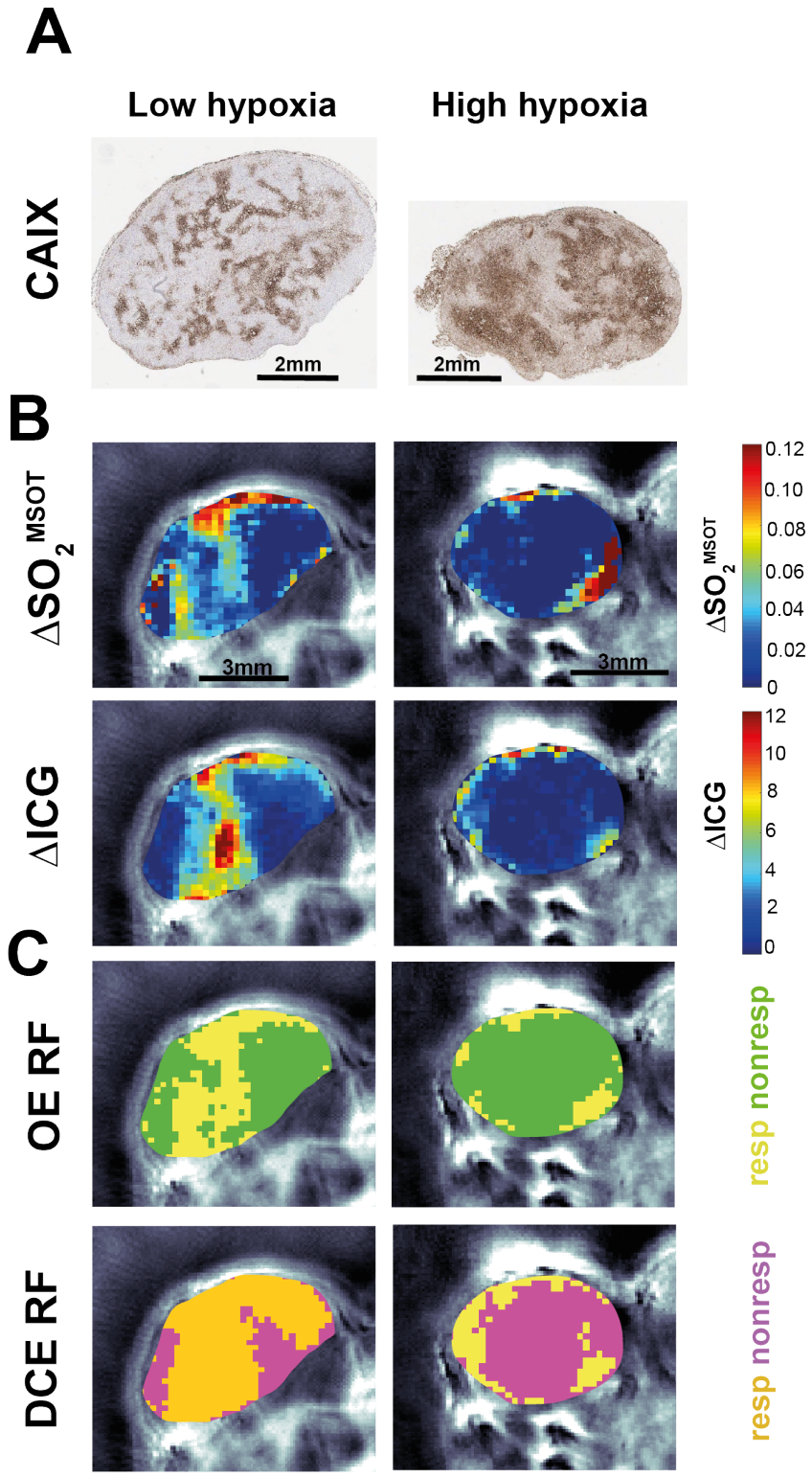

Supplementary Figure S8. **Necrotic tumours show weak OE-OT and DCE-OT response.** Representative PC3 viable (left) and highly necrotic (right) tumours, as shown in H&E stained sections (A) show differences in the amplitude of OE and DCE-OT response (B), which translate to low OE and DCE RF in the binarised response images of necrotic tumours (C).

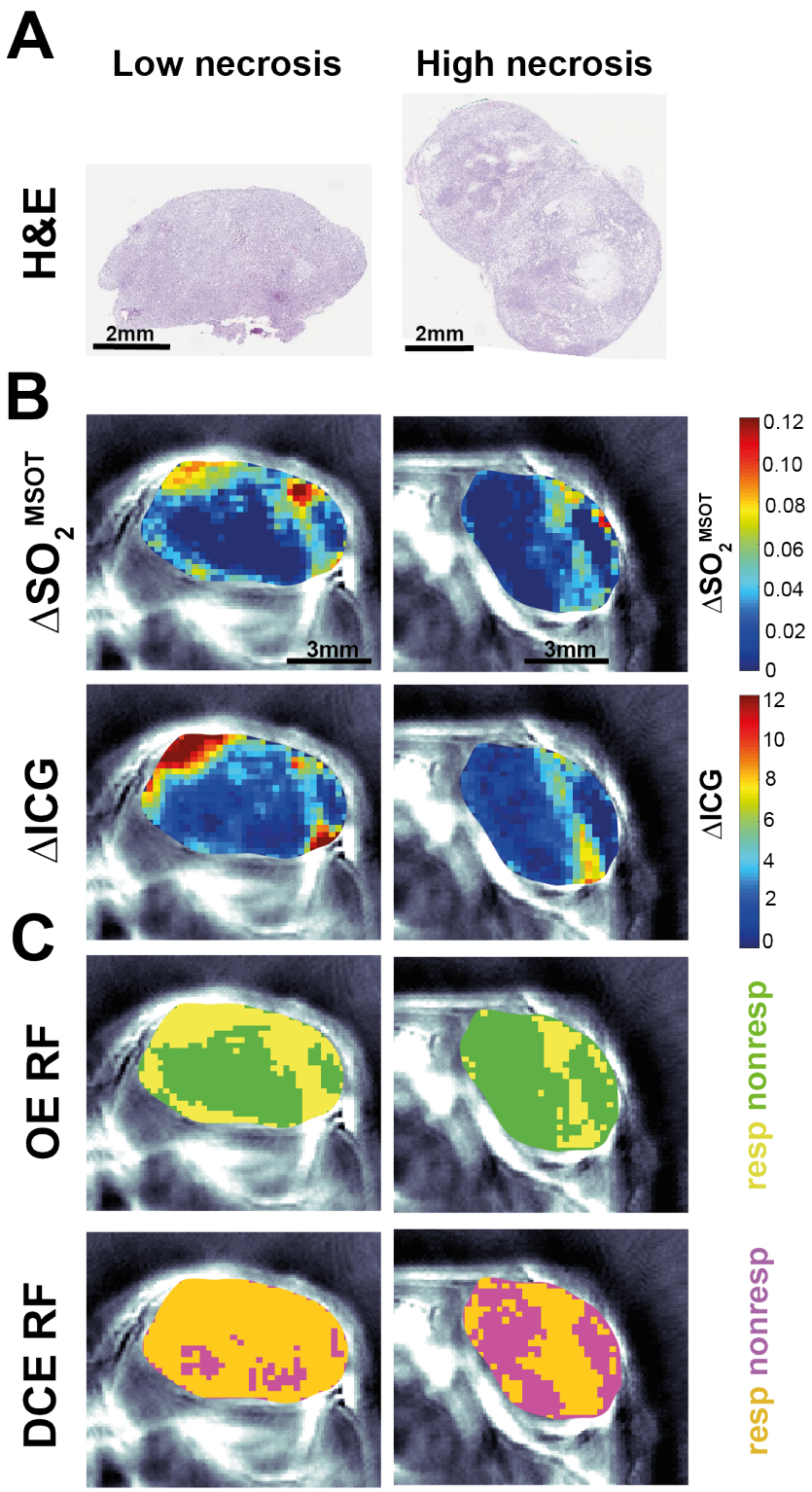

Supplementary Figure S9. **Treatment with a vascular disruptive agent causes vascular shutdown.** Vascular Disruptive Agent CA4P led to marked haemorrhage in PC3 tumours , as seen in H&E sections (A). Significant differences in in the observed haemorrhagic area (B, n=12 PC3 tumours) and smooth muscle coverage of blood vessels (C, n=12 PC3 tumours) was observed between vehicle and drug treated tumours. * $p<0.05$, ** $p<0.01$, *** $p<0.001$ by paired two-tailed t-test. Box between 25th and 75th percentile, line at median.

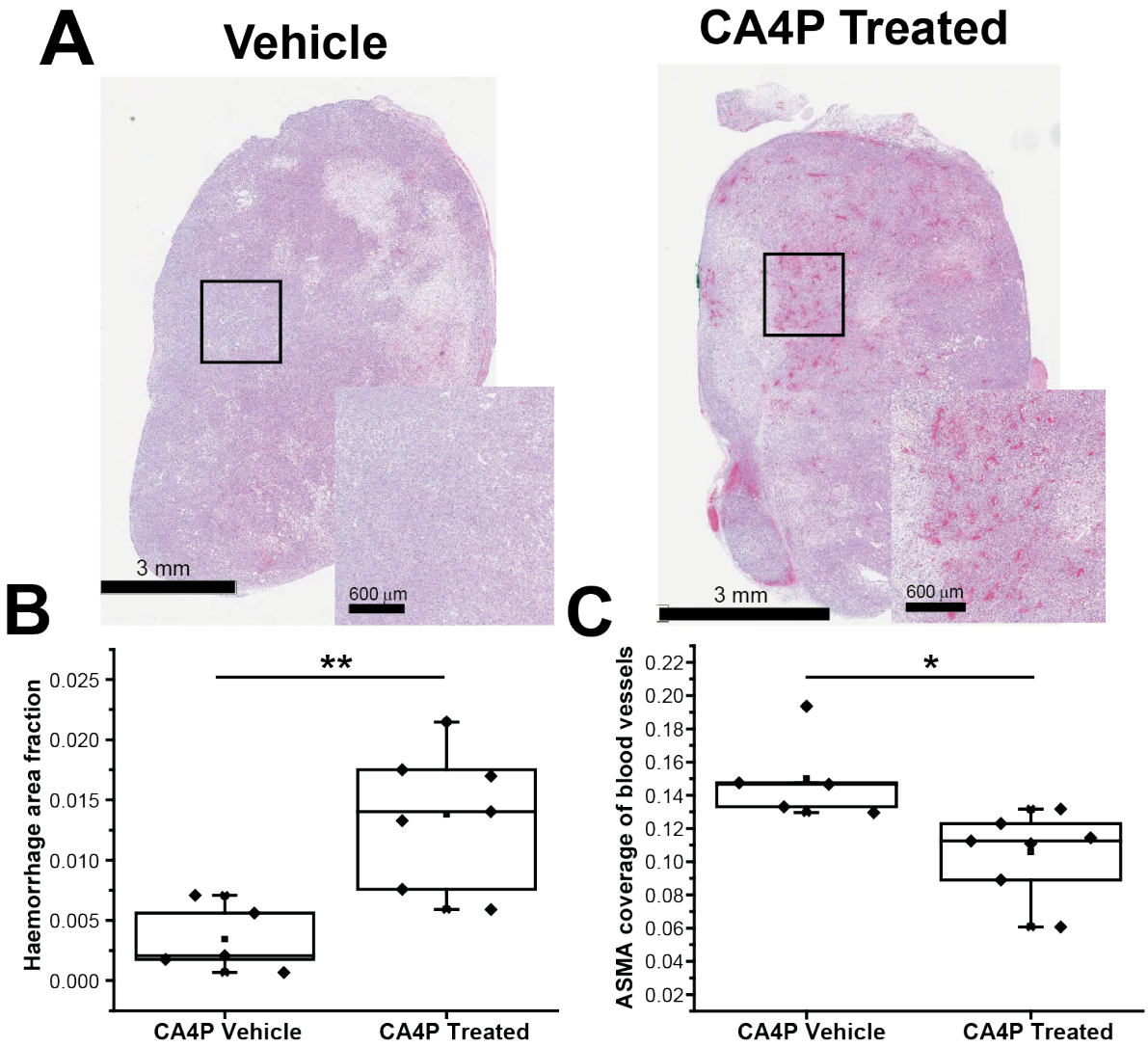

Supplementary Figure S10. **Vascular disruption causes a dramatic decrease in OE-OT and DCE-OT responses.** (A) Amplitudes of OE-OT ΔSO_2^{MSOT} (top) and DCE-OT ΔICG (bottom) decrease dramatically following treatment with the vascular disruptive agent CA4P. Averaged kinetic curves for vehicle (B) and drug treated (C) animals confirm this observation. n=5 PC3 tumours were vehicle treated, n=7 PC3 tumours received CA4P. Shaded envelope in (B) and (C) indicates standard error of the mean.

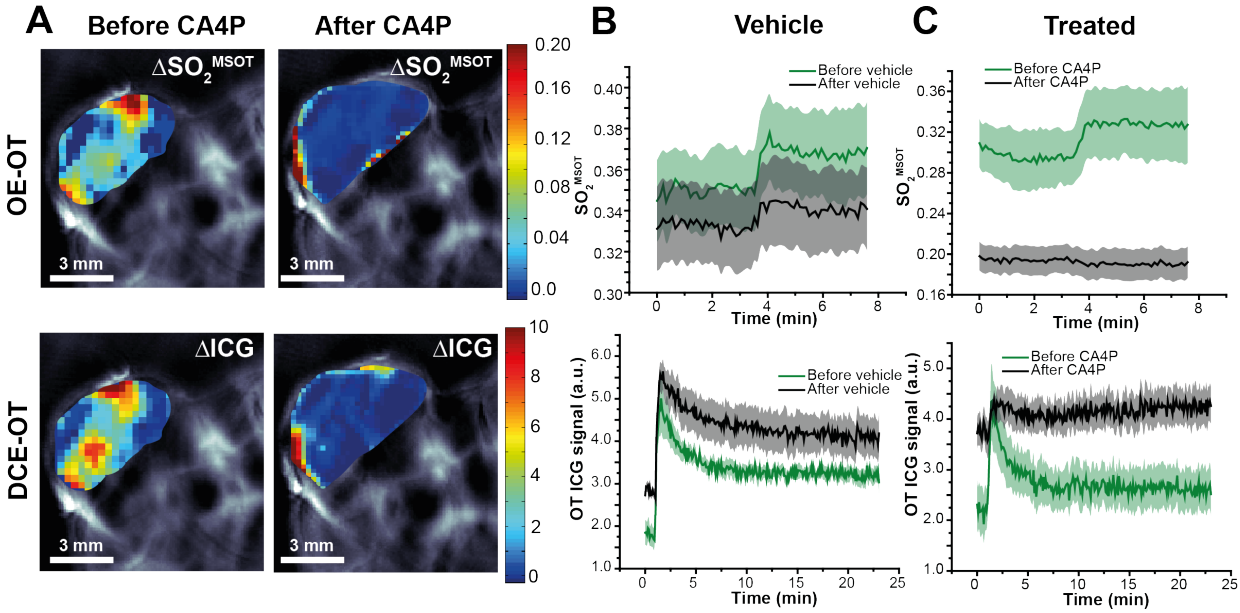

Supplementary Figure S11. **Vehicle treated PC3 tumours show no change in spatial distribution of OE and DCE response.** OE (top) and DCE (bottom) response maps show little change following vehicle treatment, contrary to the dramatic effect of the CA4P drug.